Improved Quantitation of Dynamic SPECT via Fully 4-D Joint Estimation of Compartmental Models and Blood Input Function Directly from Projections

Bryan W. Reutter, *Senior Member, IEEE,* Sang Oh, Grant T. Gullberg, *Fellow, IEEE,* and Ronald H. Huesman, *Fellow, IEEE*

***Abstract*— Quantitative kinetic analysis of dynamic cardiac single-photon emission computed tomography (SPECT) data provides unique information that can enable improved discrimination between healthy and diseased tissue, compared to static imaging. In particular, compartmental model analysis can provide quantitative measures of myocardial perfusion, viability, and coronary flow reserve. In this work we investigate whether precision of kinetic parameter estimates is improved by additional temporal regularization provided by estimating compartmental models directly from projection data, rather than using "semidirect" methods that estimate time-activity curves first and then fit compartmental models to the curves. Methods are implemented to accelerate fully 4-D direct joint estimation of compartmental models for tissue volumes and B-spline time-activity curves for the blood input and other volumes that do not obey a compartmental model. Computer simulations of a dynamic ^{99m}Tc-teboroxime cardiac SPECT study show that the additional temporal regularization provided by direct compartmental modeling results in improved precision of parameter estimates, as well as comparable or improved accuracy. Notably, for small myocardial defects the sample standard deviation of uptake and washout parameters was reduced by 17–41%. These results suggest that direct joint estimation of compartmental models and blood input function can improve quantitation of dynamic SPECT. These methods can also be applied to dynamic positron emission tomography (PET).**

I. Introduction

QUANTITATIVE kinetic analysis of dynamic cardiac single-photon emission computed tomography (SPECT) data provides unique information that can enable improved discrimination between healthy and diseased tissue, compared to static imaging. In particular, compartmental model analysis can provide quantitative measures of myocardial perfusion, viability, and coronary flow reserve [1], [2].

In this work we investigate whether precision of kinetic parameter estimates is improved by additional temporal regularization provided by estimating compartmental models directly from dynamic projection data, rather than using "semidirect" methods. Previously we developed fast methods for estimating B-spline models for time-activity curves for segmented volumes directly from projections [3]–[5]. Compartmental models were then fit to the curves. This "semidirect" approach to compartmental modeling removed parameter bias generated by artifacts that appear in conventionally reconstructed SPECT images because of projection data inconsistency and truncation of the field of view by cone-beam collimators.

In the present work, methods are implemented to accelerate fully 4-D joint estimation, directly from SPECT projections, of compartmental models for tissue volumes and B-spline time-activity curves for the blood input and other volumes that do not obey a compartmental model [these methods can also be applied to dynamic positron emission tomography (PET)]. Computer simulations show that the additional temporal regularization provided by direct compartmental modeling improves the precision of uptake and washout estimates, particularly for small myocardial defects.

This work was supported by the U.S. Department of Health and Human Services under grants R01-HL50663 and R01-HL71253, and by the Director, Office of Science, Office of Biological and Environmental Research, Medical Sciences Division of the U.S. Department of Energy under contract DE-AC03-76SF00098.

The authors are with the Department of Functional Imaging, Lawrence Berkeley National Laboratory, University of California, Berkeley, CA 94720, USA (e-mail: bwreutter@lbl.gov).

II. Spatiotemporal Projection Data Model

In the following model (which we proposed in [6] and implement and test for the first time here), the projected field of view is encompassed by $M = M_1 + M_2$ segmented volumes that contain spatially uniform activity distributions. Time-activity curves for volumes $m = 1, \ldots, M_1$ are modeled with use of B-splines, and curves for volumes $m = (M_1 + 1), \ldots, M$ are described with use of one-compartment models.

The B-spline model for the time-activity curve for volume m is

$$A^m(t) = \sum_{n=1}^{N} a_{mn} V^n(t), \tag{1}$$

where a_{mn} are model coefficients, $V^n(t)$ are B-spline basis functions [7], and N is the number of basis functions. Splines with smaller support typically are used to model rapidly changing portions of curves, while splines with larger support are used to model slow changes (e.g., [3], [8]). For convenience, the blood input volume is assigned index $m = 1$.

For the one-compartment kinetic model, the relationship between the blood input function, $A^1(t)$, and the activity in the tissue in volume m, $Q^m(t)$, is modeled to be

$$\frac{dQ^m(t)}{dt} = k_1^m A^1(t) - k_2^m Q^m(t), \tag{2}$$

where k_1^m is the uptake rate parameter and k_2^m is the washout rate parameter. For initial conditions of zero, the tissue activity is the convolution of the blood input function with a single decaying exponential:

$$Q^m(t) = k_1^m \int_0^t A^1(\tau) e^{-k_2^m(t-\tau)} d\tau. \tag{3}$$

Total activity in volume m is given by

$$R^m(t) = f_v^m A^1(t) + Q^m(t), \tag{4}$$

where f_v^m is the fraction of the volume occupied by vasculature.

The detected count rate at time t along ray i is modeled as

$$P_i(t) = \sum_{m=1}^{M_1} U_i^m(t) A^m(t) + \sum_{m=M_1+1}^{M} U_i^m(t) R^m(t), \tag{5}$$

where $U_i^m(t)$ is the spatial projection along ray i of the indicator function for volume m. Physical effects such as attenuation, geometric point response, and scatter are incorporated in $U_i^m(t)$, which is time-varying as a result of SPECT gantry motion.

The model for the projection data is obtained by integrating (5) over L contiguous time intervals that span the data acquisition from time $t_0 = 0$ to time $t_L = T$:

$$p_{il} = \int_{t_{l-1}}^{t_l} P_i(t) dt. \tag{6}$$

If the time intervals are short enough so that each segmented volume projection function $U_i^m(t)$ is approximated well by a piecewise constant function with amplitude u_{il}^m during time interval $[t_{l-1}, t_l]$, then the following approximation can be made:

$$p_{il} \approx \sum_{m=1}^{M_1} u_{il}^m \int_{t_{l-1}}^{t_l} A^m(t) dt + \sum_{m=M_1+1}^{M} u_{il}^m \int_{t_{l-1}}^{t_l} R^m(t) dt. \tag{7}$$

Substituting (1), (3), and (4) into (7) and replacing the approximation with equality, one obtains the projection data model

$$\begin{aligned} p_{il} = & \sum_{m=1}^{M_1} u_{il}^m \sum_{n=1}^{N} a_{mn} v_l^n + \sum_{m=M_1+1}^{M} u_{il}^m f_v^m \sum_{n=1}^{N} a_{1n} v_l^n \\ & + \sum_{m=M_1+1}^{M} u_{il}^m k_1^m \sum_{n=1}^{N} a_{1n} \tilde{v}_l^{mn}, \end{aligned} \tag{8}$$

where integrals of unconvolved and convolved temporal B-spline basis functions are denoted by $v_l^n = \int_{t_{l-1}}^{t_l} V^n(\tau) d\tau$ and $\tilde{v}_l^{mn} = \int_{t_{l-1}}^{t_l} \int_0^t V^n(\tau) e^{-k_2^m(t-\tau)} d\tau dt$, respectively.

The projection data model given by (8) is nonlinear in the washout rate parameters k_2^m contained in the factors $\tilde{v}_l^{mn}$ for volumes described by compartmental models, and is linear in the spline time-activity curve coefficients a_{mn} for the other non-blood-input volumes. The compartmental model uptake rate parameters k_1^m and vascular fractions f_v^m are bilinear along with the coefficients a_{1n} for the blood input function.

III. Least-Squares Criterion and Iterative Minimization Algorithm

The projection data model parameters can be estimated relatively quickly by minimizing the sum of squared differences between the measured and modeled projections:

$$\chi^2 = \sum_{i=1}^{I} \sum_{l=1}^{L} (p_{il}^* - p_{il})^2, \tag{9}$$

where p_{il}^* are the measured projections and I is the number of projection rays acquired simultaneously by the detector(s).

Previous work suggests that a slight reduction in parameter variance can be obtained at the added expense of performing a weighted fit in which the squared differences are inversely weighted by the variances of the measured projections [4].

A. Iterative Search of the Space of Nonlinear Parameters k_2^m and Joint Estimation of Other Parameters

The Levenberg-Marquardt method [9] can be used to iteratively search the space of nonlinear washout rate parameters k_2^m for values that minimize the least-squares criterion (9). Holding the blood time-activity curve coefficients a_{1n} constant while searching the washout parameter space, one can jointly estimate all other parameters as described in Section III-B. At the expense of more computation one can also include the a_{1n} in the iterative search space, rather than hold the a_{1n} constant. Similarly, one can jointly estimate the blood curve and all other spline curve coefficients as described in Section III-C, while searching the washout parameter space and either holding constant or searching for the compartmental model parameters k_1^m and f_v^m.

The following pseudocode describes an iterative parameter update strategy that was found to quickly minimize the least-squares criterion (9) for the computer simulations described in Section IV, starting at parameter values obtained from semidirect estimation:

⟨1⟩ update blood a_{1n}, non-blood a_{mn}

⟨2⟩ update k_2^m (and k_1^m, f_v^m, non-blood a_{mn})

repeat {

  repeat {

    ⟨3⟩ update blood a_{1n}, non-blood a_{mn}

    ⟨4⟩ update k_1^m, f_v^m, non-blood a_{mn}

  } (until k_1^m, f_v^m converge)

  ⟨5⟩ update k_2^m (and k_1^m, f_v^m, non-blood a_{mn})

} (until k_2^m converge)

Steps ⟨1⟩ and ⟨3⟩ require solving the linear least-squares problem described in Section III-C, while Step ⟨4⟩ involves the linear least-squares problem described in Section III-B.

Steps ⟨2⟩ and ⟨5⟩ are the most computationally intensive, because the space of nonlinear washout rate parameters k_2^m

is iteratively searched while estimates for the k_1^m, f_v^m, and non-blood a_{mn} are simultaneously updated to solve the embedded linear least-squares problem described in Section III-B. In previous work we investigated the nonlinear problem of estimating compartmental models directly from simulated projection data for which the blood input function was assumed known [10], [11], as well as directly from cardiac patient projection data for which the blood input function was estimated separately [12].

Joint estimation of linear parameters (the non-blood a_{mn}) and bilinear parameters (the k_1^m, f_v^m, and blood a_{1n}) can be accelerated by up to three orders of magnitude for typical SPECT data acquisitions that use a multi-rotation circular (or other periodic) detector trajectory. In the following, the time index $l = 1, \ldots, L$ is replaced with the indices $\{jk; j = 1, \ldots, J; k = 1, \ldots, K\}$, where J is the number of view angles per rotation and K is the number of rotations. The index k is dropped from the spatial projection factors, which are now periodic and are denoted by u_{ij}^m.

B. Accelerated Linear Estimation of the k_1^m, f_v^m, and Non-Blood a_{mn}, Given Fixed Values for the k_2^m and Blood a_{1n}

To solve for values of the k_1^m, f_v^m, and non-blood a_{mn} that minimize the least-squares criterion (9), given fixed values for the k_2^m and blood a_{1n}, one can express the projection data model (8) in matrix form as

$$\alpha \mathbf{F}^1 \mathbf{a}_1 + \sum_{m=2}^{M_1} \mathbf{F}^m \mathbf{a}_m + \sum_{m=M_1+1}^{M} (f_v^m \mathbf{F}^m \mathbf{a}_1 + k_1^m \mathbf{\Lambda}^m \mathbf{a}_1) = \mathbf{p}, \tag{10}$$

where $\mathbf{F}^m$ and $\mathbf{\Lambda}^m$ are $IJK \times N$ matrices whose $\{[i+(j-1)I+(k-1)IJ], n\}$th elements are $u_{ij}^m v_{jk}^n$ and $u_{ij}^m \tilde{v}_{jk}^{mn}$, respectively; $\mathbf{a}_m$ is an $N \times 1$ column vector whose nth element is a_{mn}; and $\mathbf{p}$ is an $IJK \times 1$ column vector whose $[i+(j-1)I+(k-1)IJ]$th element is p_{ijk}. The parameter α has been included to allow one to adjust the blood input amplitude while minimizing the least-squares criterion (9). One can then incorporate the adjusted amplitude into the original model parameters by multiplying the a_{1n} by α, dividing the f_v^m and k_1^m by α, and resetting α to one.

Equation (10) can be written more compactly as

$$\mathbf{G}\theta_g = \mathbf{p}, \tag{11}$$

where

$$\mathbf{G} = \begin{bmatrix} \mathbf{G}_1 & \mathbf{G}_2 & \mathbf{G}_3 \end{bmatrix}$$

$$\mathbf{G}_1 = \begin{bmatrix} \mathbf{F}^2 & \cdots & \mathbf{F}^{M_1} \end{bmatrix}$$

$$\mathbf{G}_2 = \begin{bmatrix} \mathbf{F}^1 \mathbf{a}_1 & \mathbf{F}^{M_1+1} \mathbf{a}_1 & \cdots & \mathbf{F}^M \mathbf{a}_1 \end{bmatrix}$$

$$\mathbf{G}_3 = \begin{bmatrix} \mathbf{\Lambda}^{M_1+1} \mathbf{a}_1 & \cdots & \mathbf{\Lambda}^M \mathbf{a}_1 \end{bmatrix}$$

$$\theta_g^{\mathrm{T}} = \begin{bmatrix} \mathbf{a}_2^{\mathrm{T}} & \cdots & \mathbf{a}_{M_1}^{\mathrm{T}} & \alpha & f_v^{M_1+1} & \cdots & f_v^M & k_1^{M_1+1} & \cdots & k_1^M \end{bmatrix}.$$

The least-squares criterion (9) then becomes

$$\chi^2 = (\mathbf{p}^* - \mathbf{G}\theta_g)^{\mathrm{T}} (\mathbf{p}^* - \mathbf{G}\theta_g), \tag{12}$$

where $\mathbf{p}^*$ is an $IJK \times 1$ column vector whose $[i+(j-1)I+(k-1)IJ]$th element is p_{ijk}^*. The vector of values for the k_1^m, f_v^m, non-blood a_{mn}, and α that minimize χ^2 is

$$\hat{\theta}_g = (\mathbf{G}^{\mathrm{T}}\mathbf{G})^{-1} \mathbf{G}^{\mathrm{T}} \mathbf{p}^*. \tag{13}$$

Details for accelerated computation of (13) are provided in [6].

C. Accelerated Linear Estimation of the Blood a_{1n} and Non-Blood a_{mn}, Given Fixed Values for the k_2^m, k_1^m, and f_v^m

To solve for values of the blood a_{1n} and non-blood a_{mn} that minimize the least-squares criterion (9), given fixed values for the k_2^m, k_1^m, and f_v^m, one can first express the projection data model (8) in matrix form as

$$\left[\mathbf{F}^1 + \sum_{m=M_1+1}^{M} (f_v^m \mathbf{F}^m + k_1^m \mathbf{\Lambda}^m) \right] \mathbf{a}_1 + \sum_{m=2}^{M_1} \mathbf{F}^m \mathbf{a}_m = \mathbf{p} \tag{14}$$

and then write (14) more compactly as

$$\mathbf{H}\theta_h = \mathbf{p}, \tag{15}$$

where

$$\mathbf{H} = \begin{bmatrix} \mathbf{H}_1 & \mathbf{G}_1 \end{bmatrix}$$

$$\mathbf{H}_1 = \mathbf{H}_{11} + \mathbf{H}_{12} + \mathbf{H}_{13}$$

$$\mathbf{H}_{11} = \mathbf{F}^1$$

$$\mathbf{H}_{12} = \textstyle\sum_{m=M_1+1}^{M} f_v^m \mathbf{F}^m$$

$$\mathbf{H}_{13} = \textstyle\sum_{m=M_1+1}^{M} k_1^m \mathbf{\Lambda}^m$$

$$\theta_h^{\mathrm{T}} = \begin{bmatrix} \mathbf{a}_1^{\mathrm{T}} & \mathbf{a}_2^{\mathrm{T}} & \cdots & \mathbf{a}_{M_1}^{\mathrm{T}} \end{bmatrix}.$$

The least-squares criterion (9) then becomes

$$\chi^2 = (\mathbf{p}^* - \mathbf{H}\theta_h)^{\mathrm{T}} (\mathbf{p}^* - \mathbf{H}\theta_h), \tag{16}$$

and the vector of values for the a_{mn} that minimize χ^2 is

$$\hat{\theta}_h = (\mathbf{H}^{\mathrm{T}}\mathbf{H})^{-1} \mathbf{H}^{\mathrm{T}} \mathbf{p}^*. \tag{17}$$

Details for accelerated computation of (17) are provided in [6].

IV. Computer Simulations

To study the accuracy and precision of jointly estimated compartmental model and blood input function parameters, 400 realizations of cone-beam SPECT projection data having Poisson noise were generated. The simulated 15 min dynamic cardiac data acquisition by a single-detector system consisted of $I = 2048$ projection rays per view angle (64 transverse $\times$ 32 axial), $J = 120$ view angles per revolution, and $K = 15$ revolutions (i.e., $L = 1800$ time intervals). The projection bins were 7 mm $\times$ 7 mm at the detector, and the detector was 30 cm from the center of the field of view. The cone-beam collimators had a hole diameter of 2 mm, a length of 4 cm, and were offset 1 cm from the detector. The focal length was 70 cm, which resulted in truncation of the field of view (Fig. 1).

Simulated spatial distributions were obtained with use of the Mathematical Cardiac Torso (MCAT) phantom [13]. The

emission phantom (Fig. 1) was composed of 128 contiguous 1.75 mm-thick slices and contained $M = 6$ volumes of interest: the blood pool, three myocardial tissue volumes (normal myocardium, septal defect, lateral defect), liver, and background tissue. Each volume was modeled to contain spatially uniform activity. Projections were attenuated using the corresponding MCAT attenuation phantom. Attenuation and geometric point response were modeled using a ray-driven projector with line length weighting [14]. Scatter was not modeled.

The simulated time-activity curves (Fig. 2) mimicked the kinetics of ^{99m}Tc-teboroxime [15]. The amplitude of the blood input function was adjusted so that about 10 million total events were detected.

Initially, time-activity curve models for all six volumes were estimated directly from noisy projection data with use of $N = 16$ B-spline basis functions spanning 15 time segments having geometrically increasing length (Fig. 3). Piecewise quadratic B-splines were used with an initial time segment length of 10 sec. The resulting curve models were continuous through their first derivative. For noiseless projections, the modeling error was less than 2%, where the error was defined to be the root mean square (RMS) difference between the simulated curve and the spline model, normalized by the RMS value of the simulated curve [3]. Compartmental models were then fit to the curves for the three myocardial tissue volumes and the liver.

These semidirect compartmental model fits were used as starting points for direct joint estimation of refined compartmental models and B-spline time-activity curves for the blood pool and background tissue [i.e., $M_1 = 2$ in (8)]. As described in Section III, the Levenberg-Marquardt method was used to minimize the least-squares criterion (9) by varying the nonlinear washout parameters k_2^m contained in the factors $\tilde{v}_l^{mn}$ in the projection data model (8), while simultaneously updating estimates for the linear (non-blood a_{mn}) and bilinear (k_1^m, f_v^m, blood a_{1n}) parameters as solutions to embedded linear least-squares problems.

On average, about three iterations of the outer loop in the pseudocode in Section III-A were required for convergence. Total computation time averaged 5.2 min per noise realization, using a 2.5 GHz Macintosh G5.

V. Results

Fully 4-D direct joint estimation of compartmental models and blood input function yielded improved precision, as well as comparable or improved accuracy, compared to semidirect estimation (Table I). Notably, for the septal and lateral defects the sample standard deviation of uptake and washout parameters was reduced by 17–41%. Bias for the jointly estimated lateral defect uptake parameter fell to 2.8%, compared to 11% for the semidirect estimate.

These results suggest that the additional temporal regularization provided by direct compartmental modeling can improve the ability to discriminate between healthy and diseased tissue, particularly for dynamic SPECT studies performed with slowly rotating gantries.

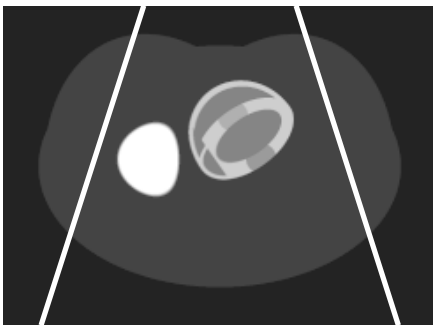

Fig. 1. Transverse cross section through the MCAT emission phantom. White lines depict data truncation resulting from the use of cone-beam collimators.

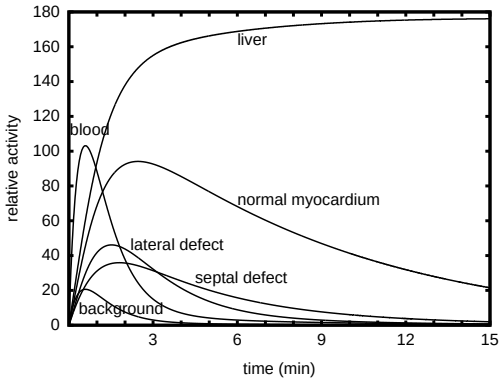

Fig. 2. Simulated time-activity curves. Myocardial and liver tissue curves were generated by one-compartment models having the blood curve as input.

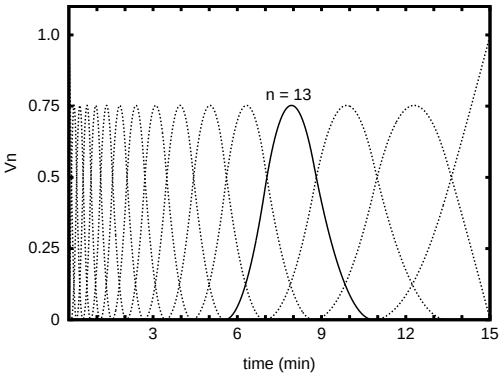

Fig. 3. Piecewise quadratic B-spline temporal basis functions used to initially model all time-activity curves. The thirteenth spline is shown as a solid curve.

VI. Future Directions

We have begun to investigate methods for modeling and estimating scatter jointly with tracer kinetic models [16]. These methods exploit the fact that the scatter distribution from a segmented volume is spatially smooth and has the same temporal kinetics as unscattered events from the volume.

To improve spatial modeling, we plan to adaptively refine the spatial segmentation and to parameterize spatially nonuniform activity distributions within the segmented volumes. For example, activity within the segmented left ventricular myocardium

TABLE I

COMPARISON OF SAMPLE MEANS AND SAMPLE STANDARD DEVIATIONS OF COMPARTMENTAL MODEL PARAMETERS ESTIMATED SEMIDIRECTLY AND JOINTLY WITH BLOOD INPUT FUNCTION (400 NOISE REALIZATIONS). THE STANDARD ERROR OF THE SAMPLE MEAN IS APPROXIMATELY 0.05 TIMES THE SAMPLE STANDARD DEVIATION. UNITS FOR UPTAKE RATE k_1^m AND WASHOUT RATE k_2^m ARE MIN^{-1}; VASCULAR FRACTION f_v^m IS DIMENSIONLESS.

		simulated value	semidirect mean ± std. dev.	direct joint mean ± std. dev.
normal myo	k_1^3	0.7	0.7001 ± 0.0061	0.6998 ± 0.0056
	k_2^3	0.15	0.1500 ± 0.0016	0.1499 ± 0.0016
	f_v^3	0.15	0.1501 ± 0.0121	0.1511 ± 0.0097
septal defect	k_1^4	0.3	0.314 ± 0.077	0.312 ± 0.061
	k_2^4	0.3	0.311 ± 0.064	0.310 ± 0.053
	f_v^4	0.1	0.100 ± 0.119	0.097 ± 0.081
lateral defect	k_1^5	0.5	0.554 ± 0.222	0.514 ± 0.132
	k_2^5	0.6	0.639 ± 0.172	0.616 ± 0.120
	f_v^5	0.1	0.075 ± 0.162	0.100 ± 0.102
liver	k_1^6	0.9	0.9001 ± 0.0050	0.9001 ± 0.0049
	k_2^6	0.002	0.0020 ± 0.0004	0.0020 ± 0.0004
	f_v^6	0.2	0.2001 ± 0.0046	0.2002 ± 0.0036

could be modeled via voxel subdivision or with use of spherical harmonic basis functions or spherical wavelets.

Future work also includes dealing with patient and organ motion. For cardiac gated studies, individual gates can be segmented and volume projection factors (i.e., u_{il}^m factors) can be calculated for each gate. This strategy can also be used for respiratory gated studies and studies in which patient or organ motion is monitored or can be detected in the projection data. For ungated studies, the segmented volume boundaries can be blurred to compensate for partial volume effects arising from cardiac contraction and respiratory motion.

ACKNOWLEDGMENT

The authors thank Dr. Benjamin Tsui at Johns Hopkins University for making the MCAT phantom available.

This work was supported by the National Heart, Lung, and Blood Institute of the U.S. Department of Health and Human Services under grants R01-HL50663 and R01-HL71253, and by the Director, Office of Science, Office of Biological and Environmental Research, Medical Sciences Division of the U.S. Department of Energy under contract DE-AC03-76SF00098.

REFERENCES

[1] G. T. Gullberg, R. H. Huesman, S. G. Ross, E. V. R. Di Bella, G. L. Zeng, B. W. Reutter, P. E. Christian, and S. A. Foresti, "Dynamic cardiac single-photon emission computed tomography," in *Nuclear Cardiology: State of the Art and Future Directions*, 2nd ed., B. L. Zaret and G. A. Beller, Eds. St Louis, MO: Mosby, 1999, ch. 11, pp. 137–187.

[2] G. T. Gullberg, R. H. Huesman, E. V. R. Di Bella, and B. W. Reutter, "Dynamic cardiac single-photon emission computed tomography using fast data acquisition systems," in *Clinical Nuclear Cardiology: State of the Art and Future Directions*, 3rd ed., B. L. Zaret and G. A. Beller, Eds. Philadelphia, PA: Elsevier Mosby, 2005, ch. 8, pp. 117–139.

[3] B. W. Reutter, G. T. Gullberg, and R. H. Huesman, "Direct least-squares estimation of spatiotemporal distributions from dynamic SPECT projections using a spatial segmentation and temporal B-splines," *IEEE Trans. Med. Imag.*, vol. 19, no. 5, pp. 434–450, 2000.

[4] ——, "Effects of temporal modelling on the statistical uncertainty of spatiotemporal distributions estimated directly from dynamic SPECT projections," *Phys. Med. Biol.*, vol. 47, no. 15, pp. 2673–2683, 2002.

[5] ——, "Accuracy and precision of compartmental model parameters obtained from directly estimated dynamic SPECT time-activity curves," *IEEE Trans. Nucl. Sci.*, vol. 51, no. 1, pp. 170–176, 2004.

[6] ——, "Fully 4-D direct joint estimation of compartmental models and blood input function from dynamic SPECT projections," in *Proceedings of the VIIth International Conference on Fully 3D Reconstruction in Radiology and Nuclear Medicine*, Y. Bizais, Ed., 2003, pp. Mo-PM3(1):1–4 (available at `http://cfi.lbl.gov/data_analysis`).

[7] R. H. Bartels, J. C. Beatty, and B. A. Barsky, *An Introduction to Splines for Use in Computer Graphics and Geometric Modeling*. Los Altos, CA: Morgan Kaufmann Publishers, 1987.

[8] T. E. Nichols, J. Qi, E. Asma, and R. M. Leahy, "Spatiotemporal reconstruction of list-mode PET data," *IEEE Trans. Med. Imag.*, vol. 21, no. 4, pp. 396–404, 2002.

[9] W. H. Press, B. P. Flannery, S. A. Teukolsky, and W. T. Vetterling, *Numerical Recipes in Fortran 77: The Art of Scientific Computing*, 2nd ed. Cambridge, England: Cambridge University Press, 1992.

[10] R. H. Huesman, B. W. Reutter, G. L. Zeng, and G. T. Gullberg, "Kinetic parameter estimation from SPECT cone-beam projection measurements," *Phys. Med. Biol.*, vol. 43, no. 4, pp. 973–982, 1998.

[11] B. W. Reutter, G. T. Gullberg, and R. H. Huesman, "Kinetic parameter estimation from attenuated SPECT projection measurements," *IEEE Trans. Nucl. Sci.*, vol. 45, no. 6, pp. 3007–3013, 1998.

[12] ——, "Kinetic parameter estimation from dynamic cardiac patient SPECT projection measurements," in *1998 IEEE Nuclear Science Symposium and Medical Imaging Conference Record*, R. Sudharsanan, Ed., 1999, pp. 1953–1958.

[13] B. M. W. Tsui, J. A. Terry, and G. T. Gullberg, "Evaluation of cardiac cone-beam single photon emission computed tomography using observer performance experiments and receiver operating characteristic analysis," *Invest. Radiol.*, vol. 28, no. 12, pp. 1101–1112, 1993.

[14] G. L. Zeng, G. T. Gullberg, B. M. W. Tsui, and J. A. Terry, "Three-dimensional iterative reconstruction algorithms with attenuation and geometric point response correction," *IEEE Trans. Nucl. Sci.*, vol. 38, no. 2, pp. 693–702, 1991.

[15] R. K. Narra, T. Feld, and A. D. Nunn, "Absorbed radiation dose to humans from technetium-99m-teboroxime," *J. Nucl. Med.*, vol. 33, no. 1, pp. 88–93, 1992.

[16] B. W. Reutter, G. T. Gullberg, and R. H. Huesman, "Spatiotemporal scatter models for dynamic SPECT," in *2004 IEEE Nuclear Science Symposium and Medical Imaging Conference Record*, J. A. Seibert, Ed., 2004, pp. 4092–4096.